

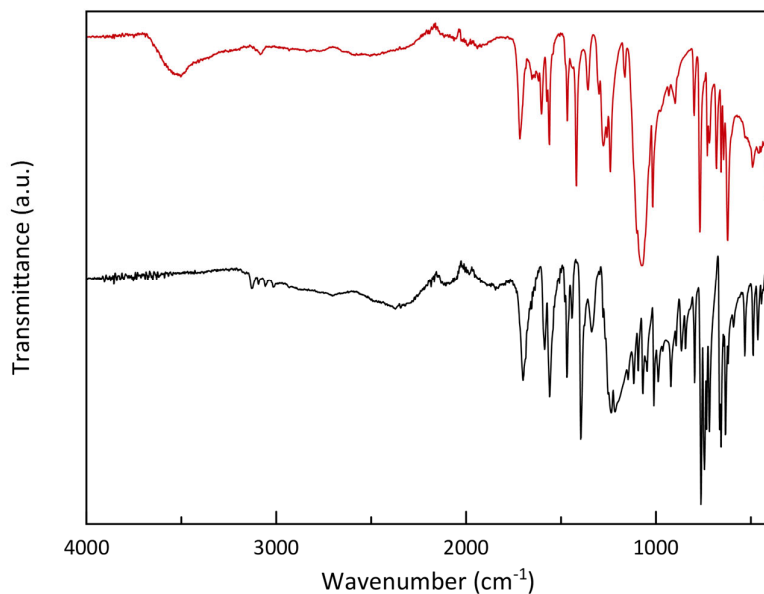
# Field-Induced Single-Ion Magnet Behavior in Nickel(II) Complexes with Functionalized 2,2':6'-2''-Terpyridine Derivatives: Preparation and Magneto-Structural Study

Francisco Ramón Fortea-Pérez <sup>1</sup>, Julia Vallejo <sup>1</sup>, Teresa F. Mastropietro <sup>2</sup>, Giovanni De Munno <sup>2,\*</sup>, Renato Rabelo <sup>1,3</sup>, Joan Cano <sup>1,\*</sup> and Miguel Julve <sup>1,\*</sup>

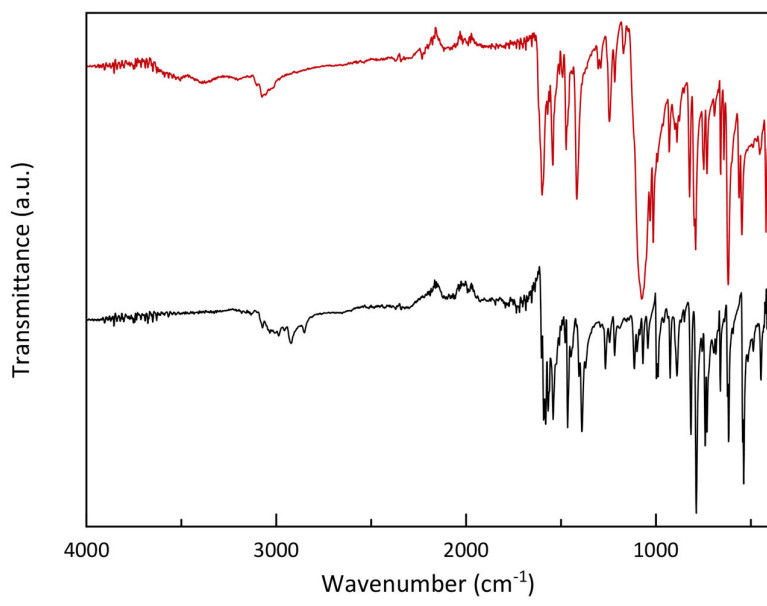
<sup>1</sup> Institut de Ciència Molecular (ICMol), Departament de Química Inorgànica, Universitat de València, 46980 Paterna, Spain; francisco.fortea@uv.es (F.R.F.-P.); julia.vallejo@uv.es (J.V.); renato.rabelo@uv.es (R.R.)

<sup>2</sup> Dipartimento di Chimica e Tecnologie Chimiche, Università della Calabria, 87036 Rende, Italy; teresafina.mastropietro@unical.it

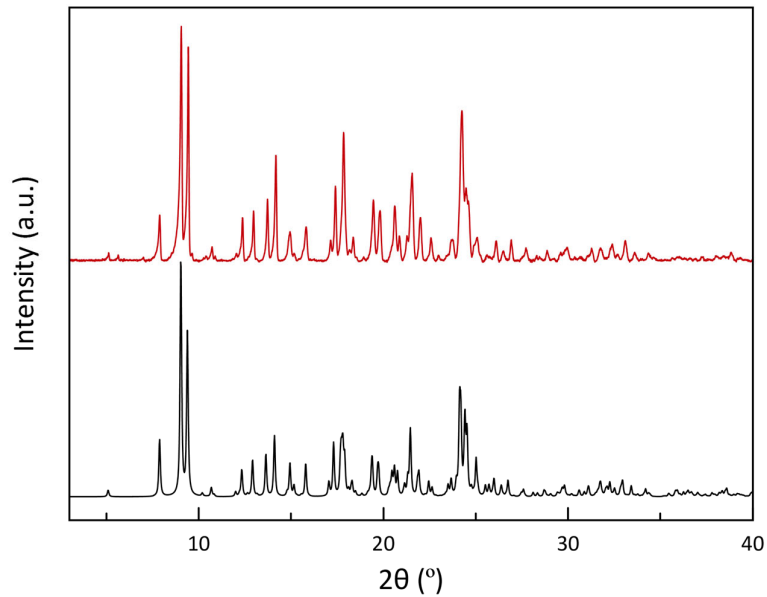
<sup>3</sup> Instituto de Química, Universidade Federal de Goiás, 74690-900 Goiânia, Brazil



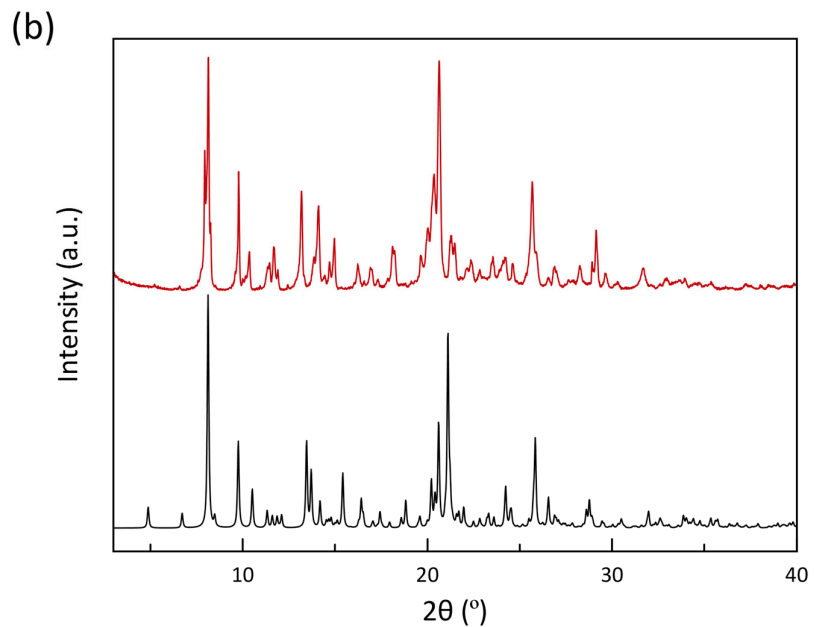
**Figure S1.** Infrared spectrum of **1** (red) compared to the ligand terpyCOOH (black).



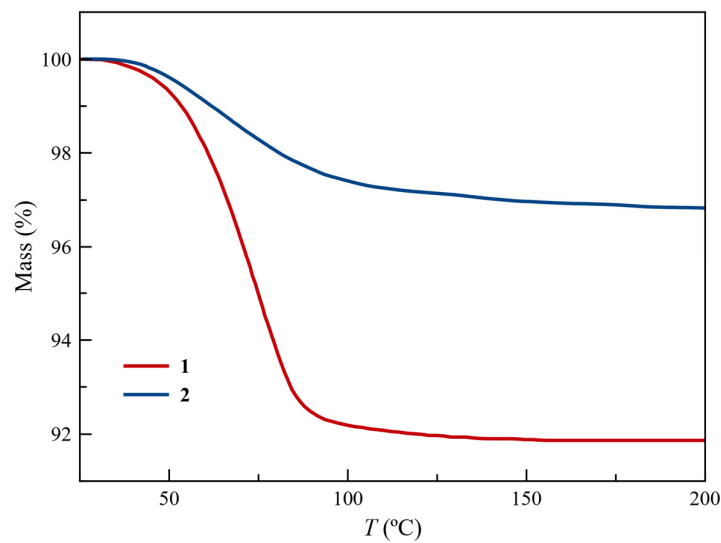
**Figure S2.** Infrared spectrum of **2** (red) compared to the ligand terpyepy (black).



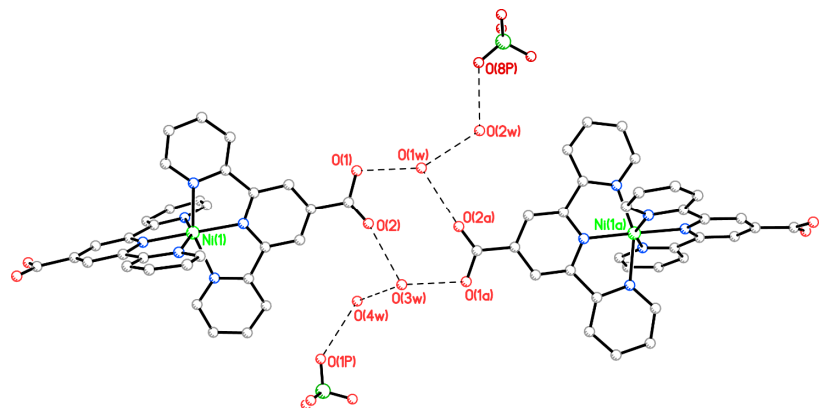
**Figure S3.** Calculated (black) and experimental (red) X-ray diffraction patterns for **1**.



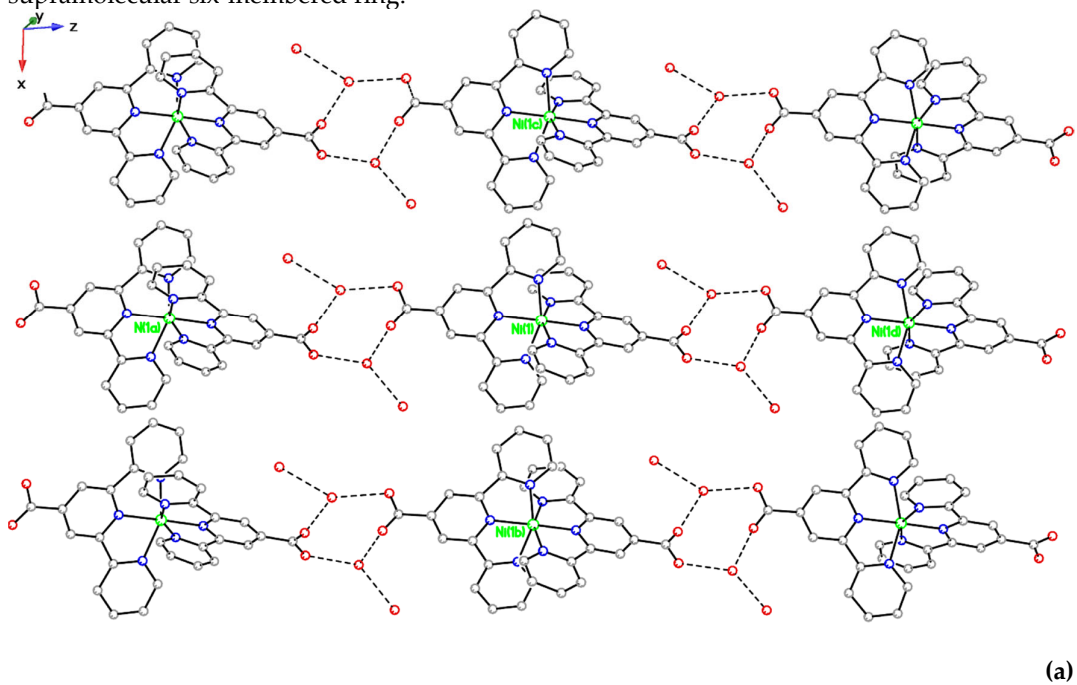
**Figure S4.** Calculated (black) and experimental (red) X-ray diffraction patterns for **2**.



**Figure S5.** Thermogravimetric behavior of **1** and **2** under a dinitrogen flow of  $100 \text{ mL min}^{-1}$  with a heating rate of  $10 \text{ }^{\circ}\text{C min}^{-1}$ .



**Figure S6.** View of the hydrogen bonding pattern in **1** illustrating the occurrence of a supramolecular six-membered ring.



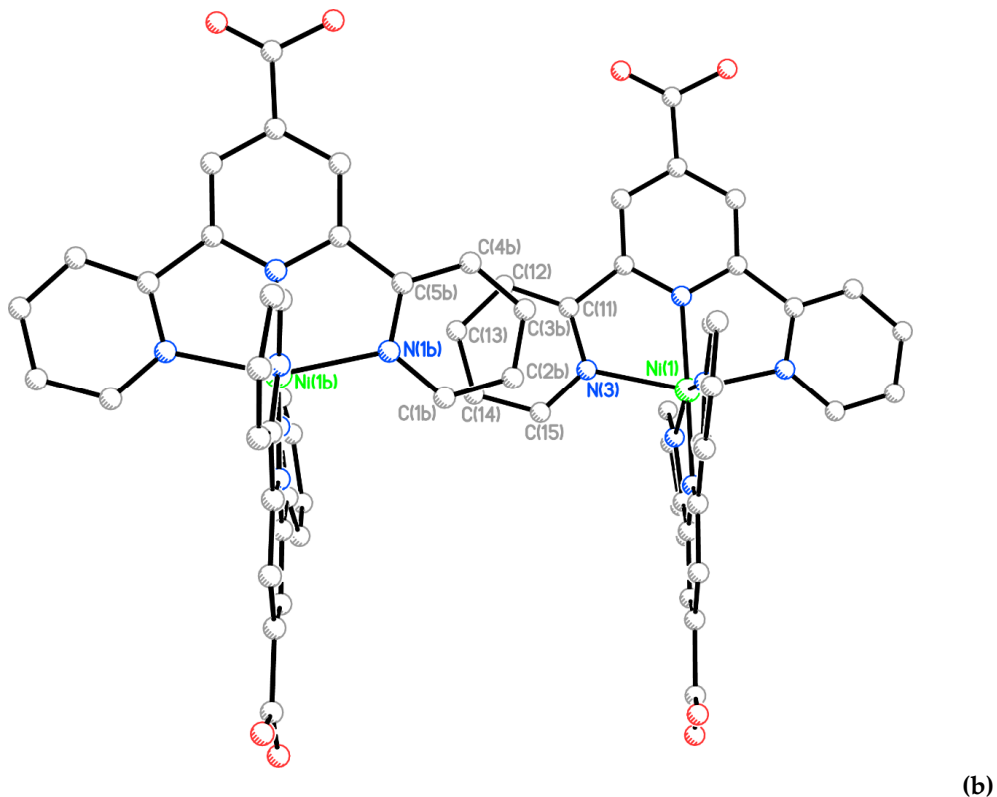
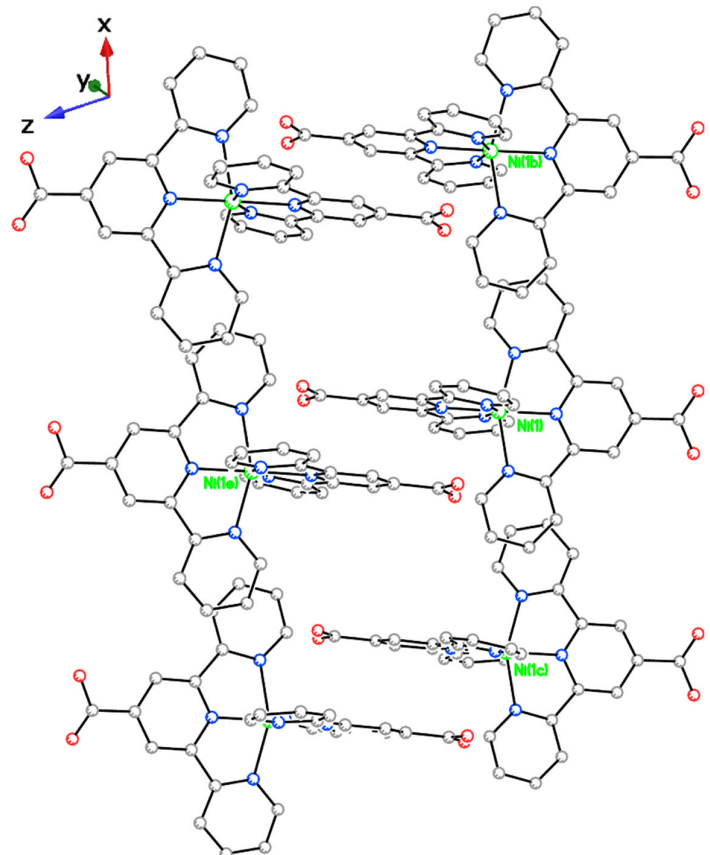
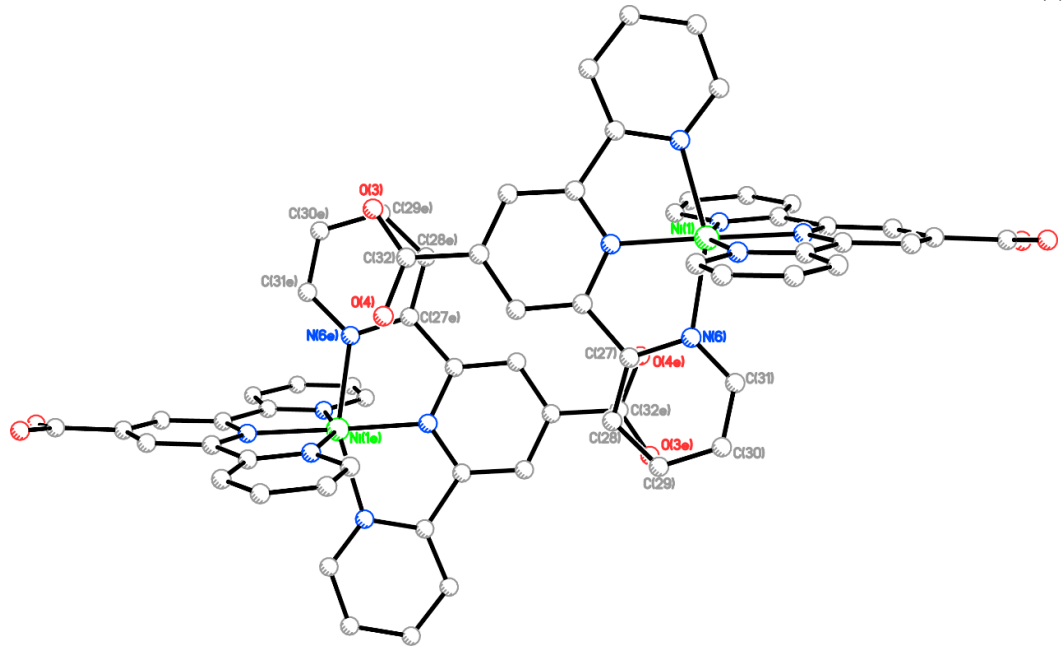


**Figure S7.** (a) Hydrogen bonding interactions along the crystallographic  $c$  axis and  $\pi-\pi$  stacking between the  $\text{N}(1)/\text{N}(3)$  pyridyl rings of one terpyCOOH ligand leading to a supramolecular 2D motif in the  $ac$  plane in **1**. (b) A detail of the  $\pi-\pi$  interactions between the outer  $\text{N}(1)$  and  $\text{N}(3)$  pyridyl rings of one ligand, which propagate along the crystallographic  $a$  axis [ $\text{N}(1)/\text{N}(3\text{b})$  and,  $\text{N}(3)/\text{N}(1\text{c})$ ; symmetry code: (b) =  $1 + x, y, z$ ; (c) =  $-1 + x, y, z$ ] in **1**.



(a)



(b)

**Figure S8.** a) and b) Views of the stacking-like interactions between the N(6) pyridyl ring of one terpyCOOH molecule and the C(32)-O(2)-O(3) carboxylic group of an adjacent terpyCOOH ligand in **1** [symmetry code:  $j(e) = 1 - x, -y, -z$ ].

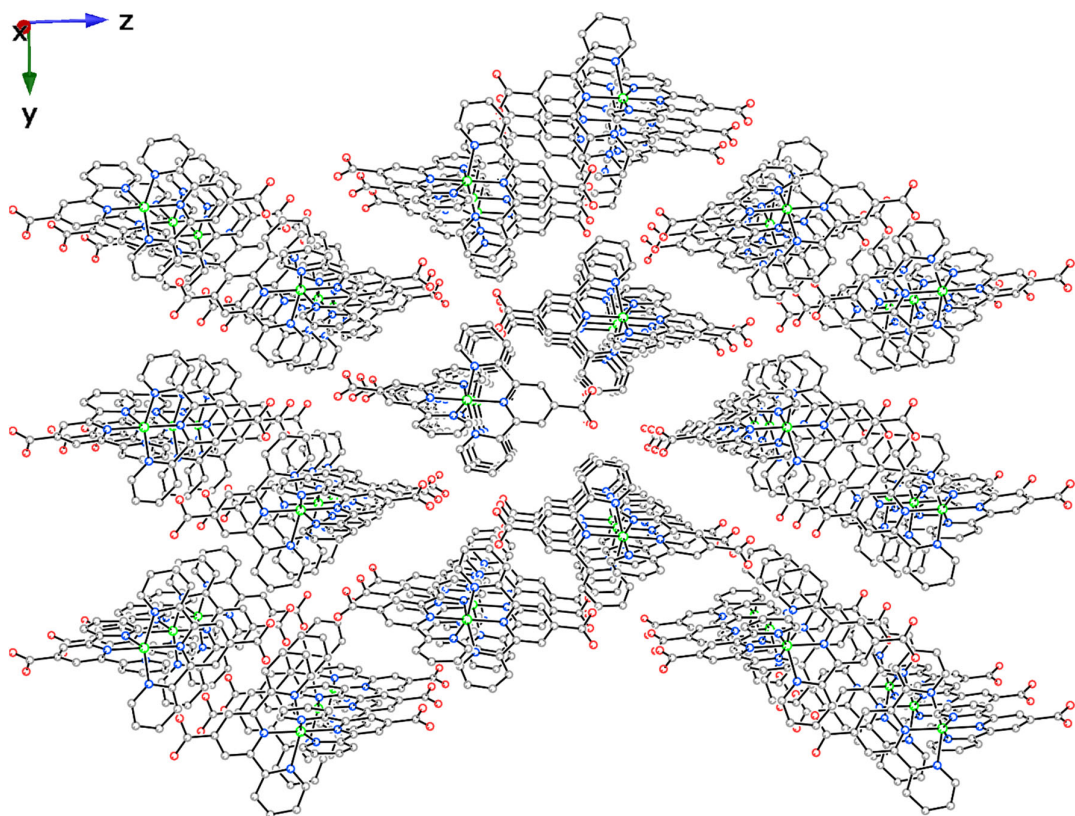


**Figure S9.** View of the supramolecular 3D arrangement in **1** supported by additional hydrogen bonds involving the water molecules of crystallization and the perchlorate anions.

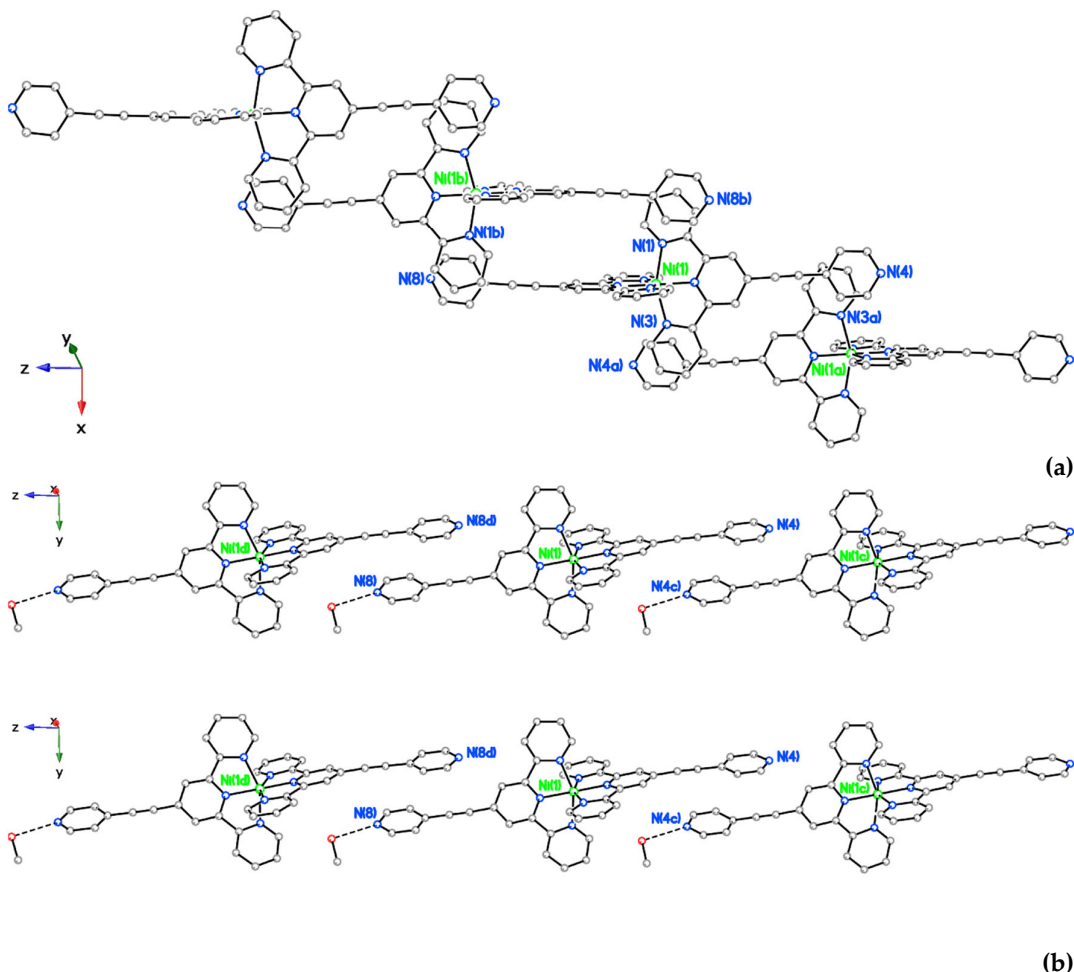


**Figure S10.** (a) A view of the supramolecular 1D motif in **2** growing along the *bc* diagonal being assembled by  $\pi-\pi$  interactions between the  $[\text{Ni}(\text{terpyepy})_2]^{2+}$  complex cations where the epoxide groups and the outer pyridyl rings of only one terpyepy ligand participate [symmetry code: (a) =  $1 - x, -y, -z$ ; (b) =  $1 - x, 1 - y, 1 - z$ ]. (b) Additional stacking interactions between the epoxide pyridyl rings containing the N(4) and N(8) atoms along the crystallographic *z* axis in **2**.

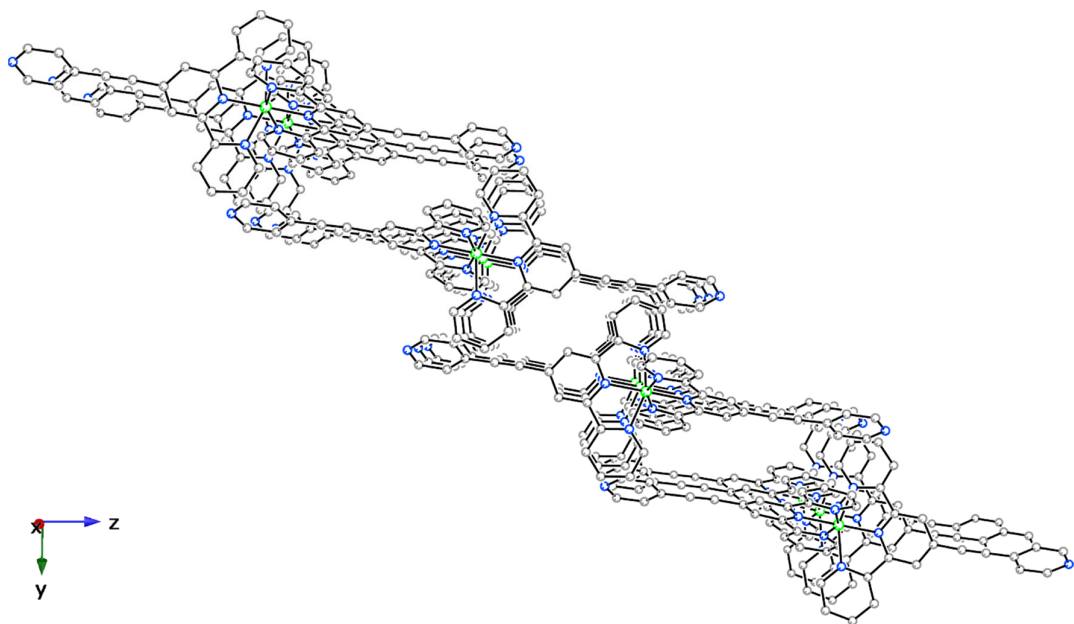


**Figure S11.** View of a fragment of the supramolecular 2D motif arising from  $\pi$ - $\pi$  interactions between the  $[\text{Ni}(\text{terpyepy})_2]^{2+}$  complex cations in **2**.

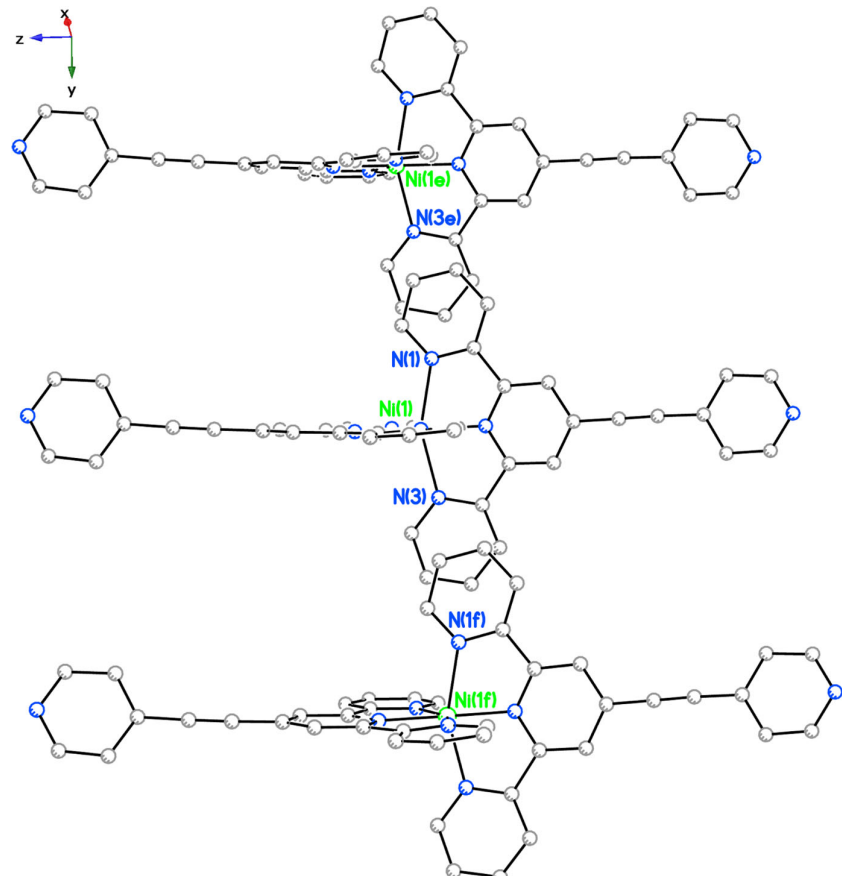


**Figure S12.**  $\pi$ - $\pi$  interactions occurring between the pyridyl rings containing the N(1) and N(3e) and N(3) and N(1f) atoms [symmetry code: (e) =  $-1 + x, y, z$ ; (f) =  $1 + x, y, z$ ] atoms along the crystallographic  $x$  axis.

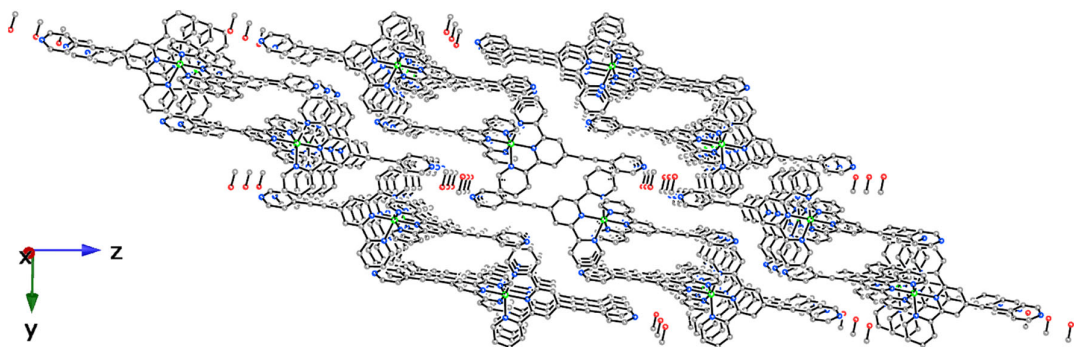


**Figure S13.** A view of the supramolecular 3D assembly in **2** showing the methanol solvent molecules arranged in small channels formed along the crystallographic *a* axis.

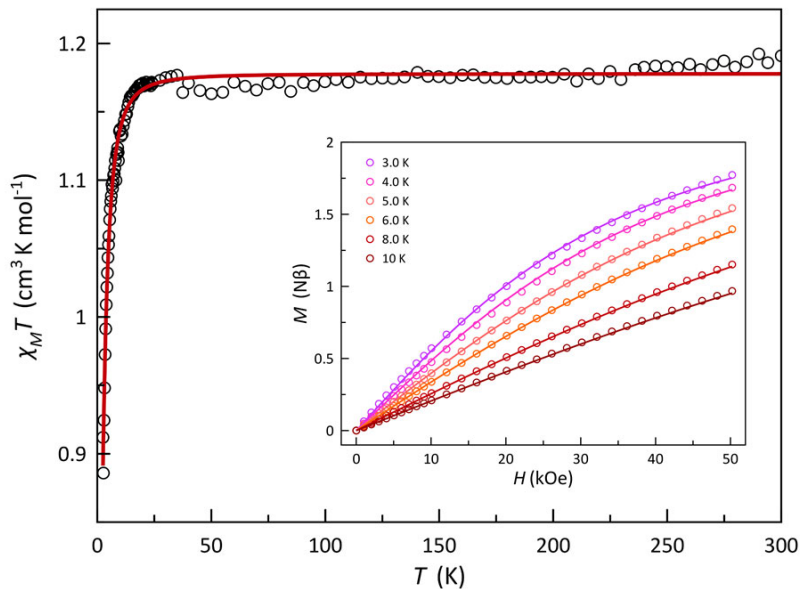
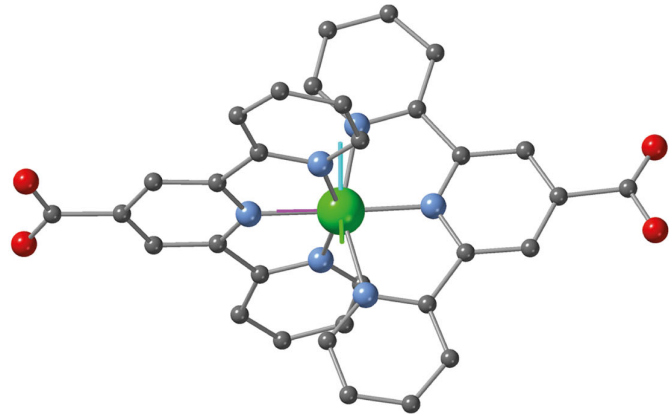


**Figure S14.**  $\chi_M T$  vs.  $T$  and  $M$  vs.  $H$  plots (inset) for **1**: (empty circles) experimental; (solid line) best-fit curves to the experimental data using the parameters reported in the text according to the *zfs* splitting approach (see text).

(a)



(b)

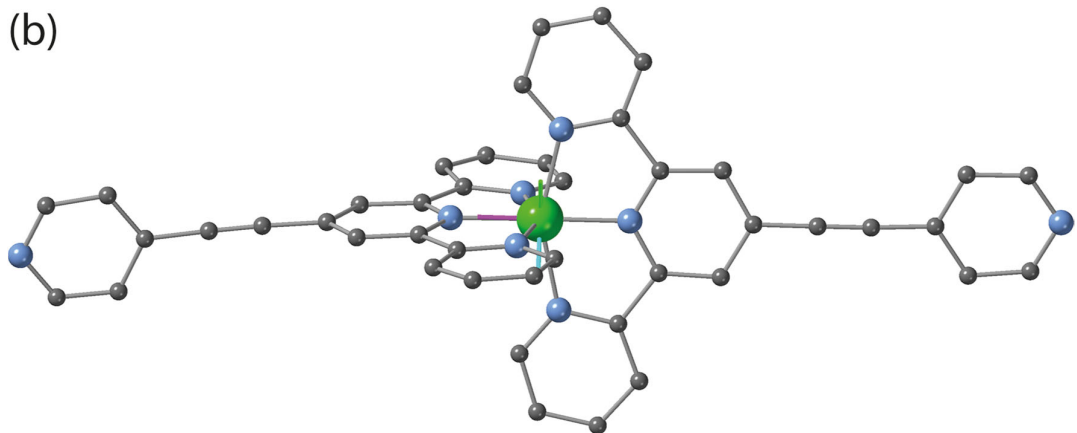


**Fig. S15.** Relative orientations of the experimental coordination environment and the calculated  $D$  tensor ( $x$  = cyan,  $y$  = green,  $z$  = magenta) for **1** (a) and **2** (b). Color code: green, nickel; light blue, nitrogen; red, oxygen; grey, carbon. Hydrogen atoms are omitted for clarity.

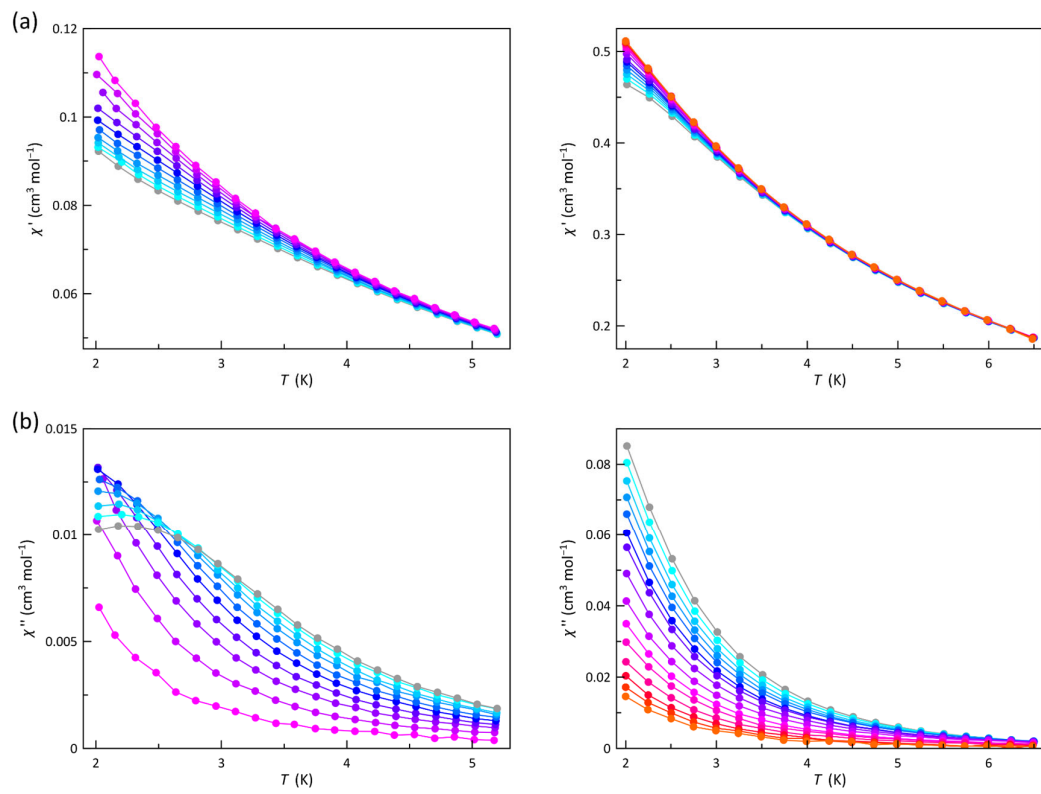


**Figure S16.** Temperature dependence of  $\chi_M'$  (a) and  $\chi_M''$  (b) of **1** (left) and **2** (right) under a static magnetic field of 2.0 and 5.0 kOe, respectively, at  $\pm 5$  Oe oscillating magnetic field in the frequency range 10.0-1.0 kHz (from gray to warmer colors).

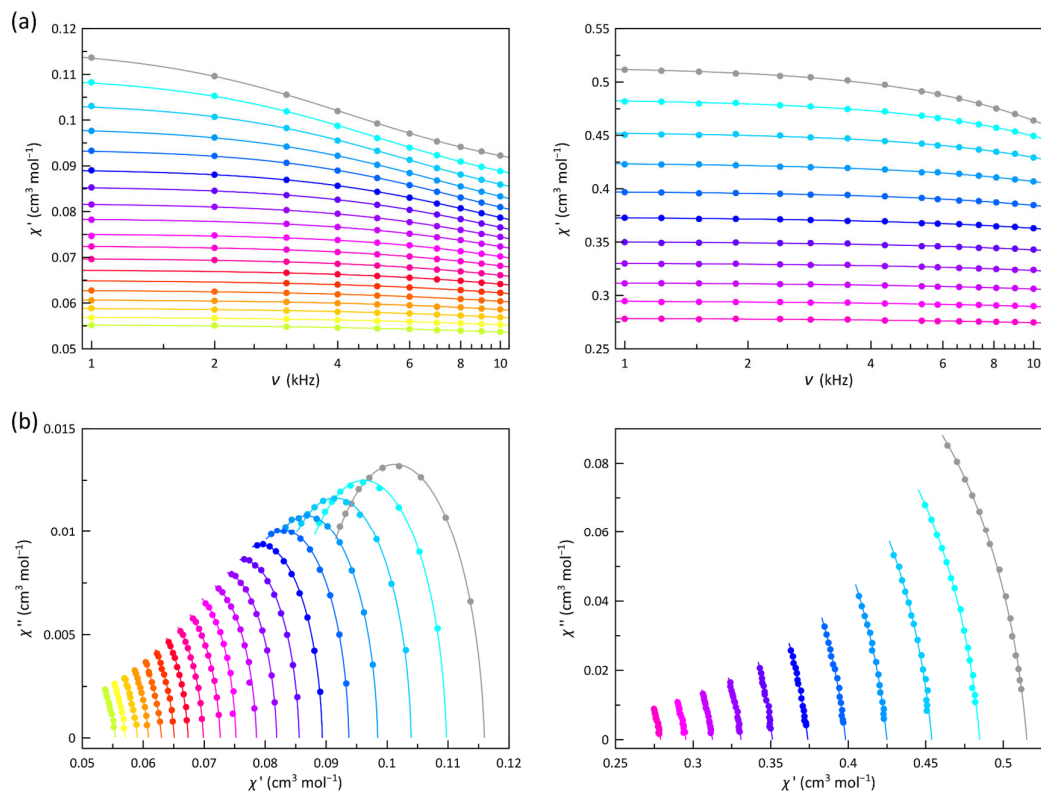


**Figure S17.** Frequency dependence of  $\otimes\chi'$  (a) and the Argand plot (b) of **1** (left) and **2** (right) under a static magnetic field of 2.0 and 5.0 kOe, respectively, at  $\pm 5$  Oe oscillating magnetic field. The solid lines are the best-fit curves obtained through the generalized Debye model.

**Table S1.** Hydrogen bonds for **1\***,&

D-H $\cdots$ A	d(D-H) [Å]	d(H $\cdots$ A) [Å]	d(D $\cdots$ A) [Å]	$\angle$ (DHA) [ $^\circ$ ]
O(4)-H(4A)...O(3W) <sup>#1</sup>	0.82	1.78	2.598(9)	176.4
O(1)-H(1A)...O(1W)	0.82	1.78	2.600(10)	174.5
O(1W)-H(1W)...O(3) <sup>#2</sup>	0.95(3)	1.85(3)	2.803(11)	175(12)
O(1W)-H(2W)...O(2W)	0.95(3)	1.92(8)	2.769(12)	148(12)
O(3W)-H(5W)...O(4W)	0.96(3)	1.90(7)	2.795(14)	155(13)
O(3W)-H(6W)...O(2)	0.96(3)	1.87(7)	2.781(12)	158(13)
O(4W)-H(8W)...O(4P) <sup>#3</sup>	0.97(3)	2.04(8)	2.93(2)	151(13)
O(2W)-H(3W)...O(8P) <sup>#4</sup>	0.96(3)	2.39(11)	3.02(3)	123(10)

\*D = donor and A = acceptor. &Symmetry transformations used to generate equivalent atoms: (#1) = x, -y + 1/2, z + 1/2; (#2) = x, -y + 1/2, z - 1/2; (#3) = -x + 2, y - 1/2, -z + 1/2; (#4) = -x + 1, y - 1/2, -z + 1/2.

**Table S2.** Energy of the calculated quartet ( $Q_i$ ) and triplet ( $D_i$ ) excited states and their contributions to the  $D$  and  $E$  values for **1** and **2** obtained from CASSCF/NEVPT2 calculations.  $D_{ss}$  is the spin-spin contribution to axial  $zfs$  parameter, and  $D_T$  and  $D_S$  stand for the sum of spin-orbit contributions coming from quartet and doublet excited states

1					2				
State	Energy <sup>a</sup>	S	$D^a$	$E^a$	State	Energy <sup>a</sup>	S	$D^a$	$E^a$
$D_{ss}$		1	+0.035	+0.011	$D_{ss}$		1	-0.031	-0.008
$D_T$		1	-7.331	-0.330	$D_T$		1	-8.351	-0.323
$D_S$		0	+1.960	-0.043	$D_S$		0	+2.254	-0.011
$T_1$	10795.6	1	-39.758	+0.007	$T_1$	10429.0	1	-41.142	-0.002
$T_2$	13062.7	1	+16.090	-6.175	$T_2$	12916.7	1	+16.215	-13.440
$T_3$	13186.5	1	+15.939	+5.933	$T_3$	12974.9	1	+15.985	+13.187
$T_4$	20039.6	1	+0.232	-0.208	$T_4$	19759.1	1	+0.311	-0.309
$T_5$	20417.1	1	+0.142	+0.114	$T_5$	20006.7	1	+0.245	+0.243
$T_6$	21361.0	1	+0.001	+0.002	$T_6$	21153.7	1	+0.001	-0.001
$T_7$	31037.8	1	+0.010	+0.010	$T_7$	30681.7	1	+0.017	+0.016
$T_8$	31318.1	1	+0.013	-0.013	$T_8$	30968.9	1	+0.017	-0.017
$T_9$	32127.6	1	-0.000	-0.000	$T_9$	31962.6	1	+0.000	+0.000
$S_1$	15911.8	0	+0.002	-0.000	$S_1$	15666.9	0	+0.001	+0.000
$S_2$	16489.7	0	-0.000	+0.000	$S_2$	16470.7	0	-0.000	-0.000
$S_3$	27026.5	0	+14.394	-0.001	$S_3$	26637.7	0	+14.581	-0.000
$S_4$	28990.6	0	-6.201	+6.097	$S_4$	28732.0	0	-6.159	+6.141
$S_5$	29218.9	0	-6.235	-6.139	$S_5$	28879.9	0	-6.169	-6.152

<sup>a</sup>Values in cm<sup>-1</sup>.